A new approach to modelling impacts on rubble pile asteroid simulants

Monthly Notices
of the
ROYAL ASTRONOMICAL SOCIETY

MNRAS **455,** 3752–3762 (2016) doi:10.1093/mnras/stv2584

A new approach to modelling impacts on rubble pile asteroid simulants

J. F. Deller,[1,2★] S. C. Lowry,[2] C. Snodgrass,[3] M. C. Price[2] and H. Sierks[1]

[1]*Max Planck Institute for Solar System Research, Justus-von-Liebig-Weg 3, D-37075 Göttingen, Germany*
[2]*Centre for Astrophysics and Planetary Science, Ingram Building, University of Kent, Canterbury CT2 7NH, UK*
[3]*Planetary and Space Sciences, Department of Physical Sciences, The Open University, Milton Keynes MK7 6AA, UK*

Accepted 2015 November 2. Received 2015 October 5; in original form 2015 February 16

ABSTRACT

Many asteroids with low bulk densities must have a rubble pile structure and internal voids. Although little is known about their internal structure, numerical simulations of impact events on these asteroids rely on assumptions on how the voids are distributed. We present a new approach to model impacts on rubble pile asteroids that explicitly takes into account their internal structure. The formation of the asteroid is modelled as a rubble pile aggregate of spherical pebbles of different sizes. This aggregate is then converted into a high-resolution smoothed particle hydrodynamics (SPH) model, accounting for macroporosity inside the pebbles. We compare impact-event outcomes for a large set of internal configurations to explore the parameter space of our model-building process. The analysis of the fragment size distribution and the disruption threshold quantifies the specific influence of each input parameter. The size distribution of the pebbles used in our model is a simple power law, containing three free parameters: the slope α, the lower cut-off radius $r_{\rm min}$ and the upper cut-off radius $r_{\rm max}$. The influence of all three parameters on the outcome is assessed in this paper. The existence of void space in our model increases the resistance against collisional disruption, a behaviour previously reported based on numerical simulations using a continuum description of porous material (Holsapple 2009). We show, for a set of asteroid collisions typical for small asteroids in the main belt, that no a priori knowledge of the exact size distribution of the pebbles inside the asteroid is needed, as the choice of the corresponding parameters does not directly correlate with the impact outcome.

Key words: methods: numerical – minor planets, asteroids: general.

1 INTRODUCTION

Most asteroids are not monolithic bodies, but consist of numerous smaller fragments and are referred to as rubble piles. Richardson et al. (2003) summarized the arguments for this conclusion, which are reinforced by the results of many recent studies: Asteroids mostly have high macroporosities of up to 70 per cent (Carry 2012); crater chains detected on the Moon and Jupiter's moons show evidence of frequent tidal disruption of small bodies (Schenk et al. 1996); resolved images taken by spacecraft show boulders consistent with a rubble pile structure for the small asteroid Itokawa (Abe et al. 2006; Saito et al. 2006) and confirm high porosities of 40 per cent for both Itokawa and asteroid Šteins (Keller et al. 2010; Jorda et al. 2012). Bodies larger than ≈100 m are therefore mainly bound by gravitation, and cohesive effects play a minor part in their long-term behaviour. This also naturally explains the apparent spin-size barrier found for asteroids with diameters larger than 150 m, that are found in general to have periods longer than 2.2 h (Pravec, Harris & Michalowski 2002; Kwiatkowski 2010). Only in the exceptional cases where single asteroids spin faster than this, as for example asteroid (29075) 1950 DA, additional cohesive forces are needed to explain the stability against mass shedding (Rozitis, MacLennan & Emery 2014).

The evolution of asteroids is largely driven by collisional processes. For the study of hypervelocity impact events, there has been some effort to model rubble pile asteroids in the hydrocodes used for this purpose. Many approaches use a homogeneous material assuming a distribution of sub-resolution voids, and equation of state and material model implement a local filling factor (e.g. Jutzi et al. 2010a). So far, the following approaches have been tried to explicitly model the internal structure of rubble pile asteroids: Benavidez et al. (2012) introduced a rubble pile model where the asteroid is represented as a spherical shell filled with an uneven distribution of basalt spheres, with radii ranging from 8 to 20 per cent of the radius of the parent body. Michel et al. (2002) and Jutzi, Michel & Benz (2010b) introduced a model for pre-fractured rubble piles, in which randomly sized fragments are connected by 'damaged' material.

★E-mail: deller@mps.mpg.de

Benz (2000) and Geretshauser, Speith & Kley (2011) investigate the collisions of inhomogeneous pre-planetesimals. These planetesimals, formed by collisional coagulation at low impact velocities, are highly porous, fluffy dust aggregates. Benz (2000) form rubble pile structures from solid spherical boulders with radii following a power law with a slope of $\alpha = 4$, requiring that a new boulder overlaps between 1 and 5 per cent with at least one other boulder. The resulting fragile structure have a filling factor of around 0.5. Geretshauser et al. (2011) describe inhomogeneities in a spherical asteroid by a random algorithm based on Gaussian distributions of the local filling factor, varying the bulk filling factor in the range of 0–0.55.

In our approach, we directly include the formation phase of rubble pile asteroids in our model. There are competing scenarios for the formation mechanism for rubble pile asteroids. Farinella, Paolicchi & Zappalà (1982) concluded that almost all asteroids are outcomes of catastrophic collisional disruption events, and that asteroids smaller than 100 km have undergone multiple shattering and disruptions. Therefore, the major constituents of a rubble pile asteroid are themselves fragments of a collision, and their size distribution and shape will be a result of the disruption event that destroyed the parent body. In the case of asteroids Eros and Itokawa, Michikami, Nakamura & Hirata (2010) endorsed this scenario by showing that the shapes of boulders found on the surface match those of fragments of impact experiments.

Alternatively, rubble pile asteroids could form by shattering initially monolithic asteroids in multiple non-catastrophic impact events. Michel, Benz & Richardson (2004) argue, that a parent body, once monolithic, would not yield internal fragments following a well-defined power law, but rather a conglomerate of randomly shaped fragment and structures.

In this paper, we focus on rubble pile asteroids that formed by gravitational accretion of fragments. In order to understand the evolution of the large-scale internal structure of these bodies, and resulting surface features, we developed a method to explicitly model the response of rubble pile constituent parts to hypervelocity impacts. Including the accretion phase, we form models of the interior of rubble pile asteroids in a three step process, as schematically shown in Fig. 1: the formation of the asteroid is modelled as a gravitational aggregation of spherical 'pebbles' that form the building blocks of our target. This aggregate is then converted into a high-resolution smoothed particle hydrodynamics (SPH) model, which also accounts for macroporosity on the surface of, and inside, the 'pebbles'. To simulate high-velocity impacts on these models, we use the SPH solver in the hydrocode AUTODYN. While hydrocodes using different discretization strategies, like the widely used iSALE code (Collins, Melosh & Ivanov 2004; Elbeshausen, Wünnemann & Collins 2009), have advantages of more accurate treatment of material interfaces, the planned usage of our model to study the long term behaviour of the ejecta profits from the more straightforward calculation of gravitational forces in the gridless SPH method.

Our approach, while unable to resolve pebbles smaller than a few times SPH resolution as characterized by the *smoothing length*, h, allows us to understand the movement of the larger pebbles inside a rubble pile asteroid. While it is known that rubble pile asteroids absorb impact energy more efficiently and are therefore more stable against disruption (see Holsapple 2009), we are able to follow the fate of the constituent pebbles *during* impact events. This allows us to follow changes in large scale internal structure of the rubble pile during the collision, and therefore connect major surface features like hills or depressions to the collisional history of the body.

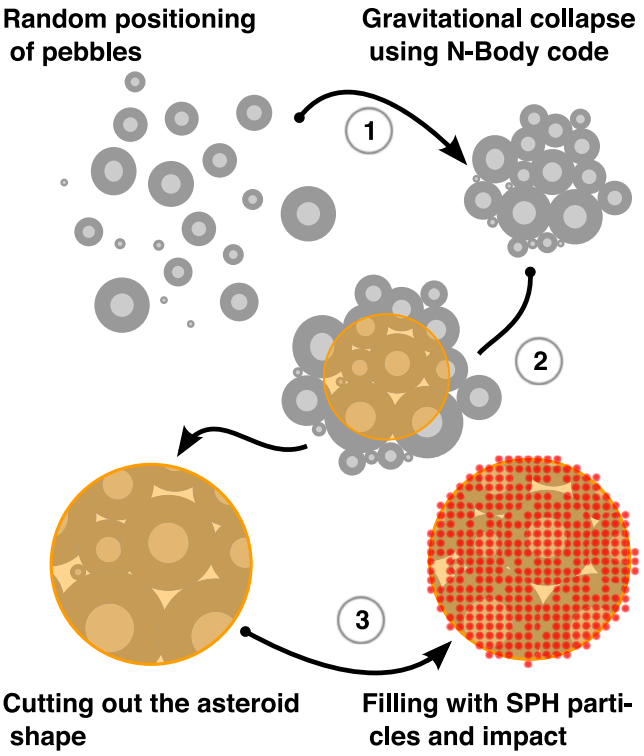

Figure 1. Schematic of our approach to model rubble pile asteroids as explained in Section 2. The pebbles are represented by hard-sphere particles, following a certain size distribution, e.g. equation (1). These pebbles are randomly distributed in space, and gravitationally collapse into an aggregate (step 1). A asteroid shape is excised (step 2), and the pebbles are filled with SPH particles following a local porosity function, e.g. equation (3) (step 3). Note that the size of the SPH particles are not to scale, and that the structure of the single pebbles is just for illustration purposes. An example of a resulting SPH impact model can be found in Fig. 4.

The aim of this paper is to assess the influence of the internal structure and size distribution of the pebbles on the outcome of impact simulations. In Section 2, we will describe our approach to creating a rubble pile simulant. We therefore choose a suitable parameter space for our test simulations using a typical collision of two small asteroids in the main belt, as described in Section 3, and discuss the results of the set of impact simulations in Section 4 and 5. Our method reproduces the expected overall response of rubble pile asteroids to hypervelocity impact events, while enabling us to trace surface changes resulting from internal reconfiguration of the major building blocks.

2 METHODS

Our approach to modelling impacts on rubble pile asteroids consists of three stages, as shown in Fig. 1: first, the rubble pile is formed as a gravitational aggregate of hard sphere pebbles which follow a defined size distribution. This aggregate is then transformed into a model suitable for SPH simulations by excising the actual asteroidal shape of interest from the gravitational pebble aggregate and exporting it into the AUTODYN hydrocode. In this step, an inner structure of the pebble itself is assumed, so porosity inside the pebbles is accounted for. Finally, the actual impact simulation using the SPH solver in AUTODYN is performed. In the following, we describe each of the steps performed in detail.

2.1 Creating rubble pile simulants

Our starting point is a set of spherical pebbles randomly distributed in space. These constituent pebbles follow a defined size distribution, that emulates the characteristics of real asteroids. In a scenario where the asteroid formed after a much larger asteroid broke up due to a major impact event, the size distribution can be inferred from impact simulations of these large-scale events. Fragment size distributions are often fitted using cumulative power laws such that $N_r(> r_s) \propto r^{-\alpha}$, where $N_r(> r_s)$ is the sum of all pebbles with radii larger than r_s, r is their radius and α is a constant describing the slope of the size distribution. Tanga et al. (1999) formulate a semi-empirical model with a power-law slope of $\alpha = 4.49 \pm 1.00$ for non-disruptive impact events resulting in asteroid family creation, and a slope of $\alpha = 4.89 \pm 0.15$ for highly disruptive events.

In a different scenario, where rubble pile asteroids form by low-speed collisions of pre-existing asteroids, the size distribution of the pebbles will follow the observed size distribution of small asteroids. Using data of the Palomar–Leiden survey (PLS; van Houten et al. 1970), a cumulative power-law slope of $\alpha = 1.95$ for bodies with diameters between 2 and 5 km were found (Kresak 1976; Davis et al. 2003). Newer surveys like the Sub-Kilometre Asteroid Diameter Survey (SKADS; Gladman et al. 2009) showed a power-law slope of $\alpha = 2.5$ for asteroids with sizes between 1 and 8 km. Values of impact crater sizes on main belt asteroid (2867) Šteins also fit in this regime, as there are found to follow cumulative power-law distribution with slope α between 1.3 and 3 (Besse et al. 2012). Also, the size distribution of boulder on asteroid (25143) Itokawa follows a cumulative power law with slope 3.1 ± 0.1 (Michikami et al. 2008).

While in both scenarios, the source material of the pebbles are likely to follow power-law distributions, it should be noted that the assumption of a power law for the pebble size distribution is just a starting point, and we need to make further assumptions to be able to use them in our code. The choice of the limiting radii (i.e. the smallest and the largest pebble) is purely based on the setup and resolution of the model: allowing pebbles larger than the radius of our target will most likely result in a monolithic target. Equally, pebbles with a size below the size of a single SPH particle will be smoothed out and behave like a monolithic target too. $r_{\rm min}$ should therefore be a least four times the resolution, as given by the smoothing length parameter h, and $r_{\rm max}$ smaller than half the target's radius. Determining the influence of these three parameters – power-law slope α, minimum radius $r_{\rm min}$ and maximum radius $r_{\rm max}$ on the outcome of an impact simulation – is one of the main aims of this study.

2.1.1 *Creating gravitational aggregates*

The aggregates are created by placing hard spherical pebbles randomly in space following the specified size distribution, and then calculating the gravitational interactions until collapse is completed. The code used is REBOUND (Rein & Liu 2012), a versatile and modular code for calculating gravitational interactions of particles.

To create the set of pebbles following the desired size distribution, we determine the radius r_i of the ith pebble from a uniformly distributed variable $u \in \mathcal{U}[0, 1]$ by

$$r_i = \left((r_{\rm max}^{-\alpha+1} - r_{\rm min}^{-\alpha+1})\, u_i + r_{\rm min}^{-\alpha+1} \right)^{\frac{1}{-\alpha+1}},\ u_i \in U = \mathcal{U}[0, 1] \quad (1)$$

The gravitational collapse is calculated in REBOUND using a very simplistic particle–particle interaction model. A coefficient of restitution of 0.4 is assumed, which allows for a quick aggregation process. An example of such a gravitational aggregate can be seen in Fig. 2. The corresponding size distribution is shown in Fig. 3. While the size distribution of the total set of pebbles follows exactly the power-law function, the size distribution of pebbles inside the excised asteroid shape is affected in two ways: first, the large pebbles, due to higher masses, seem to be over-represented in the centre of the agglomerate. Secondly, some pebbles intersect the surface of the excised asteroid shape and only part of their volume count towards the asteroids volume. The equivalent radii of these volumes are at the left of $r_{\rm min}$ in Fig. 3 and show that the overall size distribution is not significantly affected.

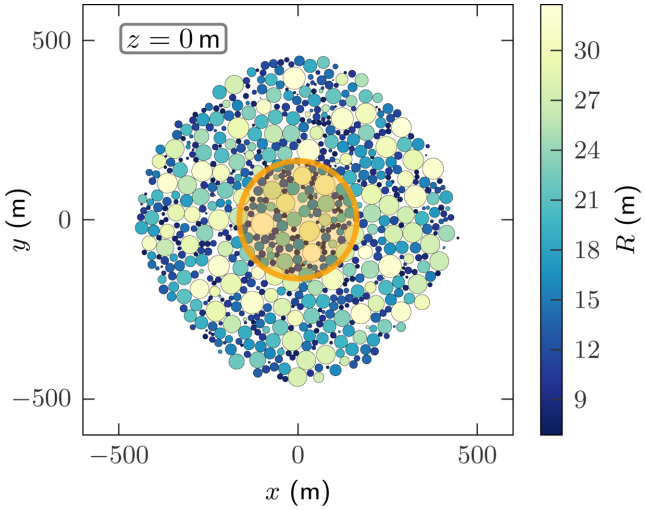

Figure 2. Central slice through a gravitational aggregate of pebbles forming a spherical asteroid of roughly 500 m radius. The power-law slope of the radius distribution is $\alpha = 2.5$, the limiting radii are: $r_{\rm min} = 6.7$ m and $r_{\rm max} = 32$ m. The size distribution of all pebbles inside the orange sphere is shown in Fig. 3. The orange sphere is the shell of an asteroid with $r = 164$ m that is excised and converted into the SPH model seen in Fig. 5 (a). The colour denotes the actual radius of the pebble, which might be larger than the radius of the circle in the intersection shown here.

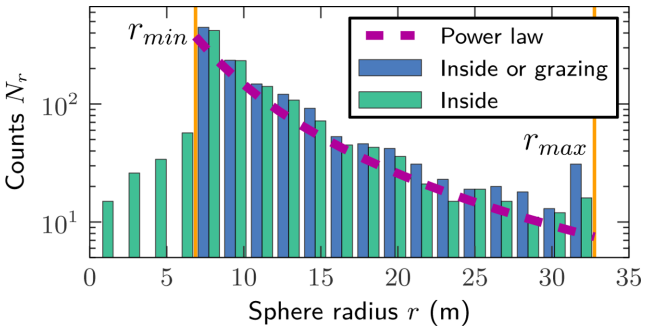

Figure 3. Distribution of radii in the gravitational aggregate shown in Fig. 2 that are inside or grazing the surface of the excised asteroid shape. The dotted line represents the power-law function $N_r \propto r^{-2.5}$. The *inside or grazing* set refers to all pebbles that touch the surface of the asteroid shape or lie inside, while for the *inside* the radii of spheres of volume equivalent to intersecting volume of pebbles at the asteroids surface and the asteroid are included and lead to the pebbles with radii smaller than $r_{\rm min}$. The limiting radii are plotted too.

2.1.2 *Converting into impact model of SPH particles*

The gravitational aggregate of pebbles formed in the first step is then transformed into an SPH model by using the location of the solid pebbles to modulate a local porosity function $P(x)$. SPH particles are placed on a grid filling the desired target shape at a position, $\boldsymbol{x}$, if a randomly chosen variable $p \in \mathcal{U}[0, 1]$ is lower than the local porosity value $P(x)$ which is given by

$$P(x) = \begin{cases} P(r_{x,i}) & x \text{ is inside pebble } i \\ 0 & \text{elsewhere} \end{cases} \quad (2)$$

where $r_{x,i} = |\boldsymbol{x} - \boldsymbol{r}_i|/r_i$ is the distance of $\boldsymbol{x}$ to the centre of the nearest pebble i at $\boldsymbol{r}_i$ of the gravitational aggregate normalized by the pebble's radius r_i. The radial porosity function $P(r_{x,i})$ describes the density profile within each pebble. Again, this is poorly constrained. It can be argued that monolithic fragments of a major disruption event will have been further fractured in the reaggregation phase, mostly on their upper layers, which would lead to pebbles that are solid in the inside and fractured (i.e. porous) on the outside. Such a profile with a bulk porosity of P_b, could be modelled using the following smooth function

$$P(r_{x,i}) = \frac{2r_{x,i}^2}{2r_{x,i}^2 - 2r_{x,i} + 1} P_\mathrm{b} \quad (3)$$

Integrated over the full normalized radius $r_{x,i} \in [0, 1]$, it returns the value for the bulk porosity, P_b, and the distribution function is strictly less than 2. Therefore, as long as $P_\mathrm{b} < \frac{1}{2}$, the overall porosity can be easily controlled by the parameter P_b.

For centimetre-sized, highly porous aggregates, Beitz et al. (2012), Weidling, Güttler & Blum (2012), and Kothe et al. (2013) showed that in further collisional evolution, material is compacted at the surface layers. A test simulation using such a profile with higher porosity in the centre of the pebbles showed a small, but significant difference in the mass excavated during a cratering event: the same impact configuration excavated 6.7 per cent of the targets mass, compared to only 2.4 per cent using the pebble porosity profile in equation (3). As the pebbles in our model are not centimetre, but metres in scale, the profile that is fragmented more at the outside seems to be more realistic. All our following simulations therefore use the profile defined by equation (3).

There are now two levels of macroporosity in the models: the voids between the spheres, and inside the material itself. This approach enables us to control the bulk porosity of our models regardless of the void space fraction in the gravitational aggregates. A cut through the central slice of a highly porous SPH model is shown in Fig. 4.

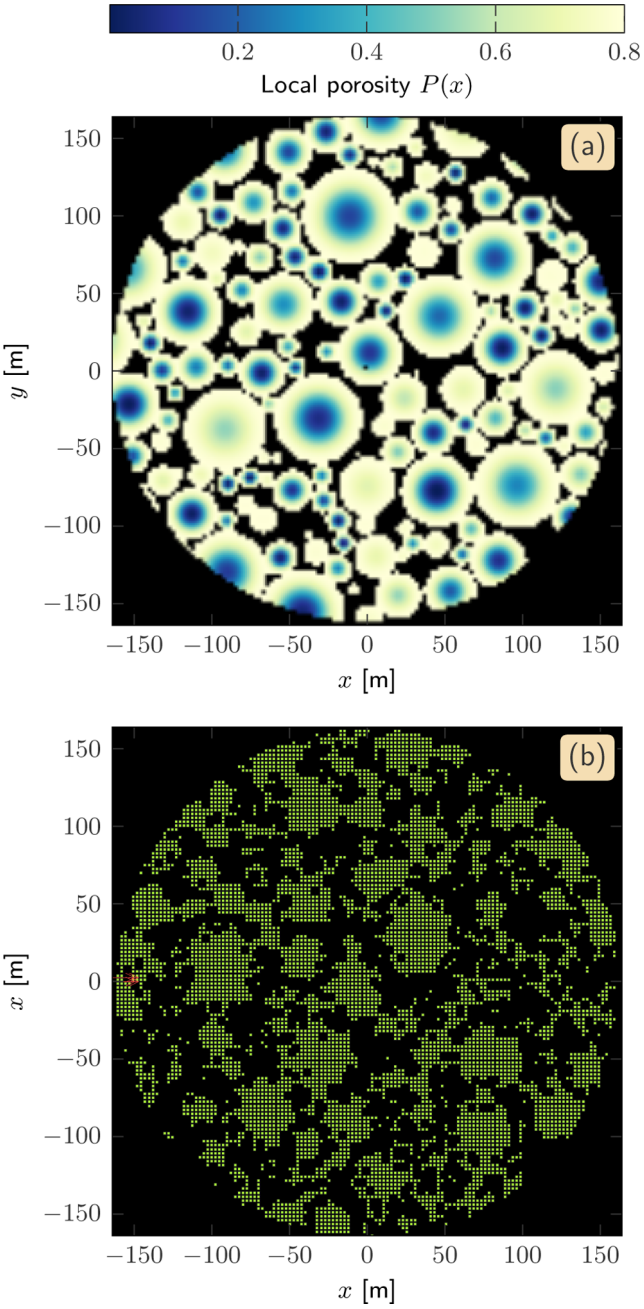

Figure 4. Map of the local porosity function $P(r_{x,i})$ described by equation (3) (top, panel a). The model was created using the gravitational aggregate in Fig. 2 in the central slice at $z = 0$ m. On the bottom in panel (b), the resulting grid of SPH points is shown. To highlight the effect, a high total void fraction in this model of $P_\mathrm{b} = 0.58$ has been chosen.

2.2 SPH simulations and material parameters

The actual impact simulations are run using AUTODYN, a 3D hydrocode. The SPH solver used here has been described by Hayhurst & Clegg (1997) and validated for hypervelocity impacts by Faraud et al. (1999) and Price et al. (2012). It has been compared to other hydrocodes using a Tillotson equation of state in a study by Pierazzo et al. (2008).

In this section, we briefly summarize the equations and parameters used in the SPH impact modelling. We follow a standard approach, as already used in many studies (e.g. Collins et al. 2004). The asteroid material in our simulations is described using a simple approach based on a Mie-Grüneisen equation of state, extended by a strength and a failure model adapted from Collins et al. (2004). All parameters are displayed in Table 1.

In the set of test simulations presented here, we used olivine as a material that is commonly found in asteroids. Olivine originates from the mantle of differentiated asteroids (Burbine, Meibom & Binzel 1996), and is therefore expected to be found in asteroids that have been created of re-aggregated material from a catastrophic disruption event.

There are not much data available about the behaviour of olivine under high-stress states. To avoid additional complexity, we use a simple linear equation of state derived from the Rankine–Hugoniot equations for jump conditions connecting physical parameters at a discontinuity like a shock. In most solids, it has been found that

Table 1. Material parameters for olivine material used in this study. See Section 2.2 for the exact formulation of the model (Marsh 1980; Collins et al. 2004).

Parameter	Symbol	Value	Unit
Reference density	ϱ_0	3214	kg m^{-3}
Gruneisen coefficient	Γ	1	None
Parameter C1	C_1	6.22	m ms^{-1}
Parameter S1	S_1	.83	None
Shear modulus	Y_{i0}	90	MPa
Coeff. internal friction, intact	μ_i	0.8	None
Limiting intact strength	$Y_{i\mathrm{lim}}$	1500	MPa
Damaged strength	$Y_{i\mathrm{d}}$	1.	MPa
Coeff. internal friction, damaged	μ_d	0.6	None
Limiting damaged strength	$Y_{i\mathrm{dam}}$	2500	MPa
Plastic strain at failure, limit	ϵ_{fc}	1.e-4	MPa
Linear coefficient	B	1.e-5	None
Limiting pressure	p_c	300	MPa
Erosion at geometric strain		0.9	none

the velocity of the impact, U_p, and the velocity of the shock front U_s, follow a linear relationship: $U_\mathrm{s} = C_1 \cdot U_p + S_1$ (e.g. McQueen, Marsh & Fritz 1967). This is used together with a Mie-Grneisen form of the equation of state (Mie 1903; Grüneisen 1912) based on the principal Hugoniot that connects every possible state described by density, shock velocity, and specific internal energy ϱ, U_s, and e reachable after a shock from the initial set of ϱ_0, U_p, and e_0:

$$p = p_H + \Gamma\varrho(e - e_H) \tag{4}$$

where

$$p_H = \frac{\varrho_0 C_1^2 \mu(1+\mu)}{(1-(S_1-1)\mu)^2} \tag{5}$$

and

$$e_H = \frac{1}{2}\frac{\varrho_H}{\varrho_0}\left(\frac{\mu}{1+\mu}\right) \tag{6}$$

Here $\mu = \frac{\varrho}{\varrho_0} - 1$ denotes the compression, and Γ the Grüneisen coefficient that describes the dependence of the pressure from the internal energy at constant volume: $\Gamma = V\left(\frac{\partial p}{\partial E}\right)_V$ and is usually set to 1.

Marsh (1980) measured shock velocities as a function of impact velocities $U_\mathrm{s}(U_p)$ for olivine. We have fitted these data, and the resulting parameters C_1 and S_1 are listed in Table 1.

We have included a more detailed strength model to describe the behaviour of material damaged by accumulated high yield stress. Strength in this model is separated into the behaviour of the intact material, where the yield strength, Y_i, is described by a Lundborg model, and failed material, where the yield strength, Y_d, is given by a Coulomb dry-friction law. The strength model is adapted from the model described in detail by Collins et al. (2004).

Damage is described by the parameter $D \in [0, 1]$ introduced by Ivanov, Deniem & Neukum (1997). D measures the plastic strain that is accumulated since the start of the simulation in each cell. The effective yield strength is then simply calculated using

$$Y = (1 - D)Y_i + DY_\mathrm{d} \tag{7}$$

In general, it would be reasonable to pre-damage material at the contact zones of the pebbles, but this has not yet been implemented into our study.

For olivine there are no data available for the parameters in this strength model. We have therefore used parameters for terrestrial granite, that have been studied by Collins et al. (2004). Given other assumptions, and since the main aims of this study are not to validate strength models of olivine, this is a reasonable starting point. Because of the difficulties in obtaining good numerical proxies for the expected asteroid material, we conducted some experiments varying the most salient parameters, Y_{i0} and μ_i. As a result, we see a strong influence of the shear strength, where a value reduced to $Y_{i0} = 9$ MPa leads to a 14 per cent smaller mass of the largest remnant fragment (M_lr). The coefficient of internal friction, on the other hand, seems not to influence the result, as a value of $\mu_i = 0$ lead to a reduction of only 3 per cent in M_lr.

To avoid additional complexity, we have not included additional sub-resolution porosity, but all porosity is provided by macroscopic voids. While this is certainly a simplification and some small-scale porosity is expected inside the pebbles, we argue that it is reasonable to concentrate on this limiting case.

3 ASSESSING THE INFLUENCE OF RUBBLE PILE STRUCTURES ON IMPACT SIMULATIONS

To validate our approach on explicitly modelling rubble pile internal structure, we have to understand the influence of all parameters controlling our model. Mainly, our model is defined by the size distribution of the pebbles used to form the gravitational aggregate. As a starting point, we have chosen to use the power law in equation (3), with three free parameters α, r_min, and r_max, to create the pebbles used for the gravitational aggregate. These three parameters are not directly constrained by observational evidence, and knowing how sensitive impact simulations are to these initial conditions is crucial to assessing the validity of such simulations in inferring anything about asteroidal collisional evolution.

We decided to run our model on a typical impact in the main asteroid belt into an asteroid of size equivalent to Itokawa. In this section, we first describe the parameters of our impact test case, and then the set of configurations of the internal structure.

3.1 Impact event and target properties

The impact event was chosen to represent a typical impact on a small asteroid in the main belt. We have chosen a spherical asteroid of radius $r_\mathrm{tar} = 164$ m, which is equivalent in volume to the rubble pile asteroid Itokawa.

We calculate simple head-on impacts on to a single target. We fix the impact velocity to 5.5 km s^{-1} as an intermediate value for relative impact velocities of two main belt asteroids that range from 4.22 km s^{-1} to (5.81 $\pm$ 1.88) km s^{-1} (Davis et al. 2003).

From scaling laws described by Holsapple (2009) we derive the impact energy expected to match the disruption threshold for the given target radius. Considering the fixed velocity, this translates into a radius of $r_\mathrm{imp} = 4$ m for a monolithic impactor, assuming the same bulk density and material as the asteroid.

Our models contain approximately 700 000 SPH particles with a smoothing length, h, of 2.54 m. The value of the bulk macroporosity for all simulations except one monolithic case is 30 per cent.

3.2 Parameter space of rubble pile simulants

The power law used in this study (equation 1) contains three free parameters: slope α, and limiting radii r_min and r_max. We test three values for the cumulative power-law slope: the observed slope in the main belt, $\alpha = 2.5$, (e. g. Gladman et al. 2009) that is similar

Table 2. Matrix of parameters to construct the pebble size distribution used in the creation of the gravitational aggregate explored in this study.

Slope α	1.95	2.5	4
Minimal radius of pebbles, $r_{\min}$ (m)	6.86	13.72	20.58
Maximal radius of pebbles, $r_{\max}$ (m)		32.8	82

to the slope for a collisionally relaxed population (Dohnanyi 1971), and the slope resulting from impact events without reaccumulation, $\alpha = 4$ (Tanga et al. 1999). For comparison with older data, we also ran simulations with $\alpha = 1.95$ (e. g. Davis et al. 2003; Kresak 1976).

Practical considerations have to be used to define the limiting sphere radii. The lower boundary is not only given by the resolution defined by the smoothing length h – each pebble should be represented by at least 32 SPH particles – but also by the fact that an aggregate too tightly packed will be indistinguishable from a monolithic material. The influence of the lower limit has therefore to be tested, and accordingly we run simulations for $r_{\min} = 6.86$ m, 13.72 m and 20.58 m, which corresponds to multiples of 2.5, 5.5 and 8 times the smoothing length h. The upper limit should be chosen so that a single sphere is considerably smaller than the asteroid itself. We have decided to test for $r_{\max} = 1/5 \cdot r_{\text{tar}}$ and $r_{\max} = 1/2 \cdot r_{\text{tar}}$. All parameter values tested are listed in Table 2.

4 COMPARING OUTCOMES OF SIMULATIONS

To assess the influence of the three parameters discussed, we have conducted numerical simulations for each point in the parameter matrix in Table 2. Additionally, we have conducted more detailed experiments on a subset of these parameters, described as Sets (a) and (b), and compared to two non-rubble pile test cases (Sets c and d). All experimental configurations are described in Table 3. As a representative example, two impact simulation outcomes for equal parameters of the slope α and $r_{\min}$, but differing in maximum radius $r_{\max}$ are shown in Fig. 5. To compare the outcomes of a large number of simulations, we define various metrics. In the following, we will discuss these metrics and the results of our simulated test cases.

4.1 Influence on the fragment size distribution and mass of the largest remnant

One natural metric is the fragment size distribution, and the relative mass of the largest remnant fragment to the body's initial mass. Although it is reasonable to use this to compare different simulations in this paper, it is more difficult to compare our results to other researchers' simulations, or observational data on asteroid families, as we do not calculate the gravitational aggregation that will follow after the disruptive impact event. The determination of the fragment size distribution is done using AUTODYN. In AUTODYN, a fragment is defined as a conglomerate of SPH particles that are all connected within a smoothing length, h, within which failure did not occur (Ansys Inc 2012).

The fragment size distribution is only helpful if it does not directly reflect the size distribution of the pebbles that formed the gravitational aggregate used to construct the model. We check this by examining the outcome of our set of test calculations: if there is a direct dependency, this should be reflected by a strong correlation of the model parameters and the largest remnant fragment. We have tested the change in slope of the cumulative fragment size distribution for four simulation setups described as Sets (a)–(d) in Table 3, two of which (Sets a and b) have been created using the rubble pile model discussed here (see Fig. 6). While they obviously

Table 3. Compilation of simulated impact configurations. Sets (a)–(d) are specific configurations referred to in the text. The three parameters of the pebble size distribution define the characteristics of the gravitational aggregate (see Section 2.1.1). The impactor radius defines the impact energy, as all impactors had a velocity of 5.5 km s^{-1}. The metric denotes the quantity used to compare a set of simulations. The mass of the largest remnant fragment, M_{lr}, can be derived for every simulation, while the disruption threshold Q^*_S is the energy at which M_{lr} is exactly 50 per cent of the target's mass. For more details, please refer to Section 4. The largest set of simulations is experiment 1, the complete matrix of power-law parameters to test the influence of the configuration of the gravitational aggregate. The results are discussed in Section 4. In experiment 2, we determine the error margin caused by the arbitrarily chosen impact location on the inhomogeneous target. The result is discussed in Section 4.1. Experiment 3 is testing the response of our rubble pile model in impact simulations compared to simple monolithic targets. This is discussed in Section 5.

	Pebble size distribution			Impactor		
	α (1)	$r_{\min}$ (m)	$r_{\max}$ (m)	r_{imp} (m)	Metric	Result in figure
Experiment 1: Influence of the gravitational aggregate parameters.						
	All permutations of α, $r_{\min}$ and $r_{\max}$ in Table 2			4	M_{lr}	10, 11, 9
Experiment 2: Testing influence of the exact impact location						
Set (a)	1.95	6.86	32.8	4	M_{lr}	7
Set (b)	4	6.86	32.8	4	M_{lr}	7
Experiment 3: Testing rubble pile model against monolithic targets						
Set (a)	1.95	6.86	32.8	2 to 8	Q^*_S	8 (5, 6)
Set (b)	4	6.86	32.8	2 to 8	Q^*_S	8 (5, 6)
Set (c)	Monolith, random macroporosity			2 to 8	Q^*_S	6, 8
Set (d)	Monolith, no macroporosity			2 to 8	Q^*_S	6, 8

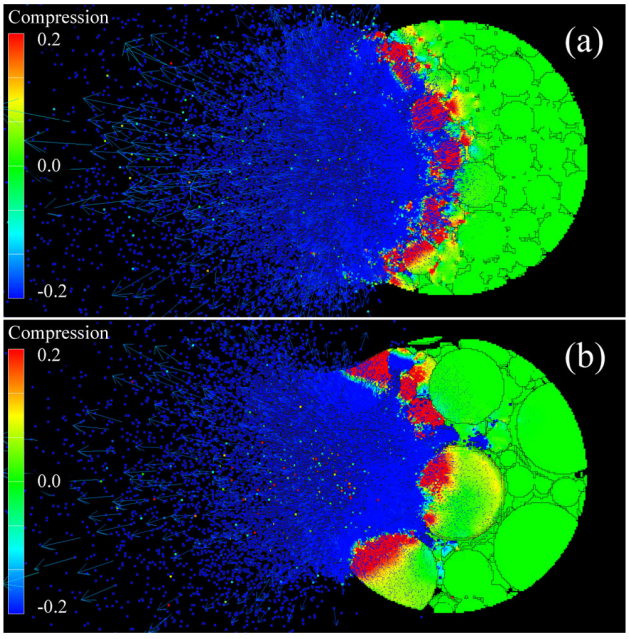

Figure 5. Distribution of material compression in impact simulations for two different internal structures after 2.8 seconds. Model (a), top was created using the gravitational aggregate shown in Fig. 2 ($\alpha = 2.5$, $r_{\min} = 6.86$ m and $r_{\max} = 32$ m). Model (b), bottom was created using an aggregate differing in the maximum radius of the pebbles used ($\alpha = 2.5$, $r_{\min} = 6.86$ m and $r_{\max} = 82$ m). There is currently no surface regolith included, but this will be added in further studies.

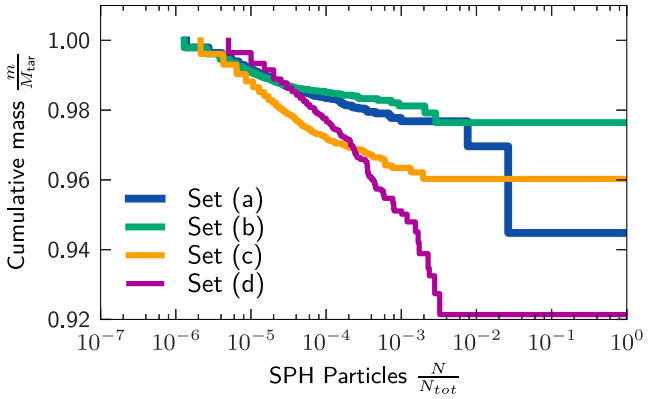

Figure 6. Cumulative distribution of fragment size for four different simulation setups: Set (a) $\alpha = 1.95$, $r_{min} = 6.86$ m, $r_{max} = 32.8$ m; Set (b) $\alpha = 4$, $r_{min} = 6.86$ m, $r_{max} = 32.8$ m; Set (c) Random porosity; Set (d) No porosity. All impacts have been calculated using an impactor of $r_{imp} = 4$ m at 5.5 km s^{-1}.

differ in the mass of the largest remnant fragment, they also differ in the characteristic of the slope. For both models that do not include the internal rubble pile structure described in this paper, but rather small, unconnected voids leading to the same macroporosity of 30 per cent (Set c) or no voids at all (Set d), the slope is much steeper than in the cases of our rubble pile model (Sets a and b). The slope for Set (a) is steeper than the slope in Set (b), while the power-law slope used to create the gravitational aggregates had been −1.95 and −4.00, respectively. This indicates that the initial slope of the pebble size distribution and the resulting fragment size distribution are not identical.

To quantify the influence of the impact location on the mass of the largest remnant fragment, we did a series of impact simulations on identical target configuration. At a randomly picked impact site, there are two extreme cases: either the impactor hits a large pebble, or the impactor will hit a void between pebbles. In Fig. 7, we show that the mass of the largest remnant fragment differs by not more than 4 per cent, with a standard deviation of roughly 1 per cent. Therefore, the typical error for each value of the mass of the largest remnant fragment in the following discussion can conservatively be regarded as ±2 per cent. Interestingly, this does not seem to depend on the exact pebble configuration at the impact zone.

4.2 Influence on the specific disruption energy threshold Q_S^*

While material strength usually means a measure of what kind of stress or strain states a certain material is able to withstand, we can also define a strength of a whole body to withstand disruption at a certain impact energy. This empirical value is usually given by the parameter, Q_S^*, defined as

$$Q_S^* = \left.\frac{E_{\rm kin,imp}}{M_{\rm tar}}\right|_{M_{\rm lr}=50\,{\rm per\,cent}\,M_{\rm tar}} \quad (8)$$

which is the normalized impact energy $\frac{E_{\rm kin,imp}}{M_{\rm tar}}$, at which the mass of the largest remnant, $M_{\rm lr}$, is exactly half the mass of the target, $M_{\rm tar}$. This denotes the transition from the cratering regime to disruption regime of the target body.

An additional complexity is the reaccumulation of ejected material. For bodies larger than a few hundred metres, the gravitational forces are able to prevent shattered fragments from dispersing (Holsapple 2009). In this so-called gravitational regime, the specific energy required to disrupt the asteroid increases with asteroid radius, and is given by Q_D^* as the specific energy at which the largest remnant after the reaccumulation has exactly 50 per cent of the target's mass. We do not take into account any reaccumulation, but as our target has a radius of just $r_{\rm tar} = 164$ m, we are just at the transition between strength and gravity regimes, and therefore Q_S^* and Q_D^* will not differ significantly.

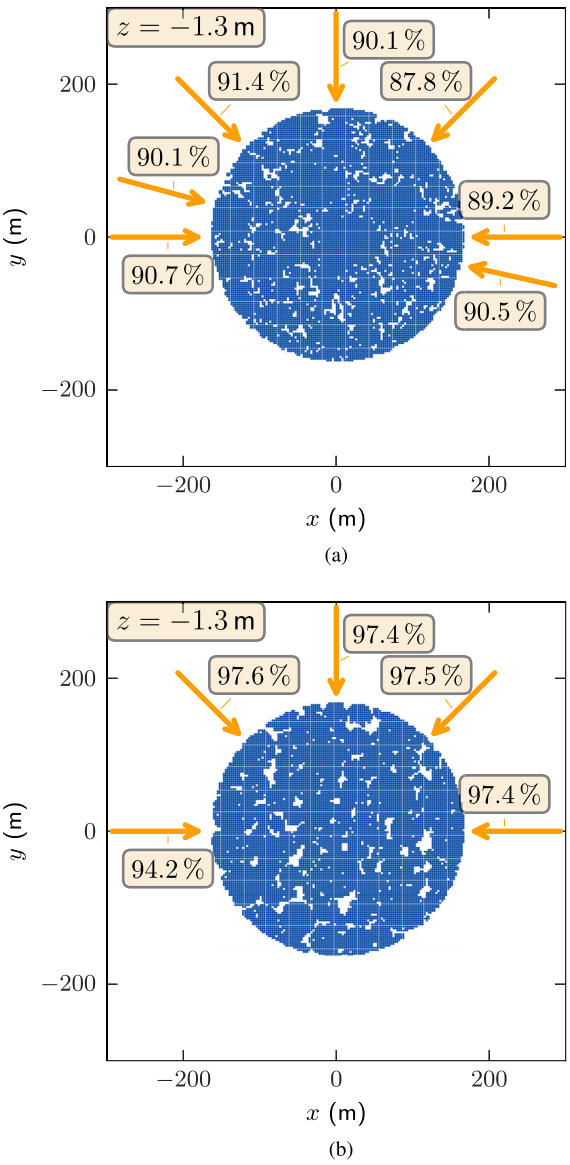

Figure 7. Relative mass of the largest remnant fragment for different impact locations on two different asteroid models. The impactor was a monolithic asteroid with $r_{\rm imp} = 4$ m at a velocity of $v_{\rm imp} = 5.5$ km s^{-1}. This allows an estimate on the error assigned to resulting largest remnant masses for individual simulations. (a) This model was created using the parameters $\alpha = 4$, $r_{\rm min} = 13.72$ m and $r_{\rm max} = 82$ m. (b) This model was created using the parameters $\alpha = 1.95$, $r_{\rm min} = 6.8$ m and $r_{\rm max} = 32.2$ m.

In Fig. 8, the largest remnant fraction as a function of the specific impact energy for four different target configurations is shown. For set (d), the one that includes no voids at all, there is a sharp transition from the cratering regime to the disruption regime at $Q_S^* = 1.29 \times 10^6$ erg g^{-1}. This sharp transition is known from laboratory-scale experiments for the disruption of non-porous targets and has been reproduced by other simulations (Benz & Asphaug 1999). For all three cases that include void space, i.e. the

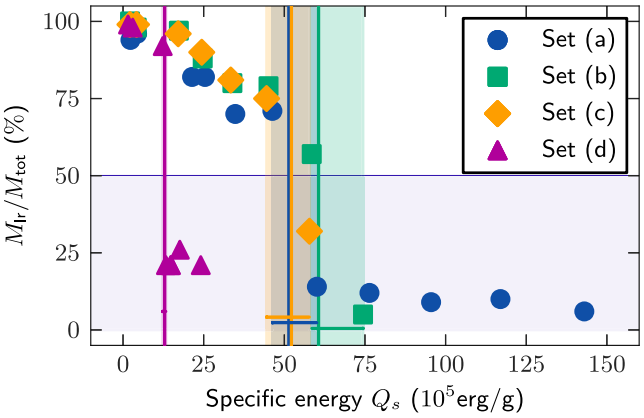

Figure 8. Specific impact energy plotted against the relative mass of the largest remnant for four different settings 30 s after impact. Set (a) $\alpha = 1.95$, $r_{min} = 6.86$ m, $r_{max} = 32.8$ m; Set (b) $\alpha = 4$, $r_{min} = 6.86$ m, $r_{max} = 32.8$ m; Set (c) Random porosity; Set (d) No porosity. The vertical lines denote the linear interpolated position at which the largest remnant has 50 per cent of the target's mass, or Q^*_S, the shaded regions show the enclosing interval.

models created using our rubble pile model (Sets a and b), as well as the model using randomly distributed void space (Set c), this sharp transition is smoothed, and shifted towards higher specific energies. Therefore, void space actually strengthens the asteroids, a behaviour observed in numerical experiments before (Holsapple 2009).

For all models including void space, the transition from cratering to disruption regime is observed at around 5×10^5–7.5×10^5 erg g^{-1}. This is slightly stronger than the value of 1×10^5 erg g^{-1} found for rubble pile aggregates by Benz (2000). However, Benz (2000) calculated impacts with a mass ratio of 1, while in our simulations the mass of the impactor is negligible to the mass of the target. Also, they consider impact velocities of just a few times the escape velocity, while in our case this ratio is around 4×10^5. Still, one of the central results of the paper by Benz (2000), that a high mass ratio leads to a more efficient energy transfer into the target and therefore to easier disruption for equal specific impact energies, is confirmed by our results.

To formulate a generalized disruption criterion as a function of mass ratio, impact angle and impact velocity, Leinhardt & Stewart (2011) formulate the disruption criterion in terms of an equivalent equal mass impact energy, $Q^*_{RD\,1:1}$, called the principal disruption curve. The authors observe a linear relation between $Q^*_{RD\,1:1}$ and an effective radius defined by $R^3_{C1} = (M_{tar} + M_{imp})/((4/3)\pi\rho_1)$ where $\rho_1 = 1000$ kg m^{-3} is the reference density. This linear relationship is characterized by a constant offset c^* to the specific gravitational binding energy. The authors find a value of $c^* = 5 \pm 2$ to be representative for small bodies in the gravitational regime, which they define as bodies larger than 300 m. In the simulations discussed in our paper, e. g. $v_{imp} = 5.5$ km s^{-1}, $r_{imp} = 4$ m, $r_{tar} = 164$ m, and $\rho_b = 2249$ kg m^{-3}, the effective radius is $R_{C1} = 214$ m. If the disruption threshold is read from Fig. 8 as $Q^*_S \approx 5.5 \times 10^6$ erg g^{-1}, than the equivalent equal mass impact energy is $Q^*_{RD\,1:1} = 2102.5$ erg g^{-1} assuming near-perfect energy scaling ($\bar{\mu} = 0.37$; see Leinhardt & Stewart 2011 for details). The expected value from the principal disruption curve assuming $c^* = 5$ is $Q^*_{RD\,1:1} = 387.2$ erg g^{-1}, clearly showing that the simulations in this work are still governed by strength effects and do not belong to the gravity regime.

A study by Jutzi et al. (2010a) focusses on the transition from strength to gravity regime for solid bodies as well as bodies containing sub-resolution voids. Scaling laws derived from numerical simulations at six sizes ranging from 3 cm to 100 km using an impact incidence angle of 45° and $v_{imp} = 5$ km s^{-1} give an expected disruption threshold for the target size discussed here of $Q^*_D = 3.05 \times 10^6$ erg g^{-1} and $Q^*_D = 1.89 \times 10^6$ erg g^{-1} for porous and solid material, respectively. This is in good agreement with the values found in this paper, as seen in Fig. 8: $Q^*_D = 5.5 \times 10^6$ erg g^{-1} and $Q^*_D = 1.29 \times 10^6$ erg g^{-1} for porous and solid material, respectively. Our rubble pile model seems to be slightly more resistant against disruption, but it is not clear how much of this difference is attributed to different material model formulations and parameters.

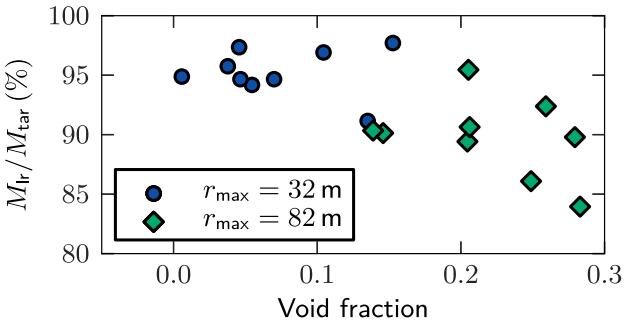

Figure 9. Relative mass of the largest remnant as a function of the void fraction in the gravitational aggregate for all simulation configurations described in Table 3, experiment 1.

5 RESULTS – SENSITIVITY TO MODEL PARAMETERS

One of the main objectives of this study is to asses the influence of the three free parameters used to create gravitational aggregates in our model – the power-law slope α, the limiting radii r_{min} and r_{max}– on the outcome of impact events. We have conducted numerical experiments for all combinations of these three parameters found in Table 2. As the inner structure of our asteroid models is controlled only by the power-law parameters used, we do not directly control the void fraction defined as the space in between the pebbles and the ratio of overall asteroid volume. Instead the overall bulk porosity P_b is equal to 30 per cent in all models. Therefore, Fig. 9 shows that models with larger pebbles ($r_{max} = 82$ m) keep more void space open, while smaller pebbles ($r_{max} = 32$ m) fill the voids. This geometric effect causes a higher void fraction if there are more large pebbles, while the pebbles will have less internal porous space. The figure also shows that a higher void fraction increases the mass excavated by the same impact energy. This effect is discussed later.

In Figs 10 and 11, the resulting mass of the largest remnant fragment for each internal configuration after a calculated impact event with an impactor speed of 4 m s^{-1} is shown. The following observations can be made:

The larger the void fraction, the smaller the mass of the largest remnant fragment M_{lr} (see Fig. 9): As the bulk porosity is constant, a larger void fraction means more *connected* voids rather than smaller, distributed voids. The larger pebbles themselves contain less porosity, and therefore behave more like a solid material that has a lower resistance against collisional disruption, or in other words a lower disruption energy Q^*_S (see Fig. 8). Through the solid larger pebbles, energy is transmitted into the centre of the asteroids more readily, additionally weakening the body.

For small $r_{min} = 6.9$ m, there is less dependence on the decrease in strength for larger r_{max} (Fig. 11b): This might be because this case

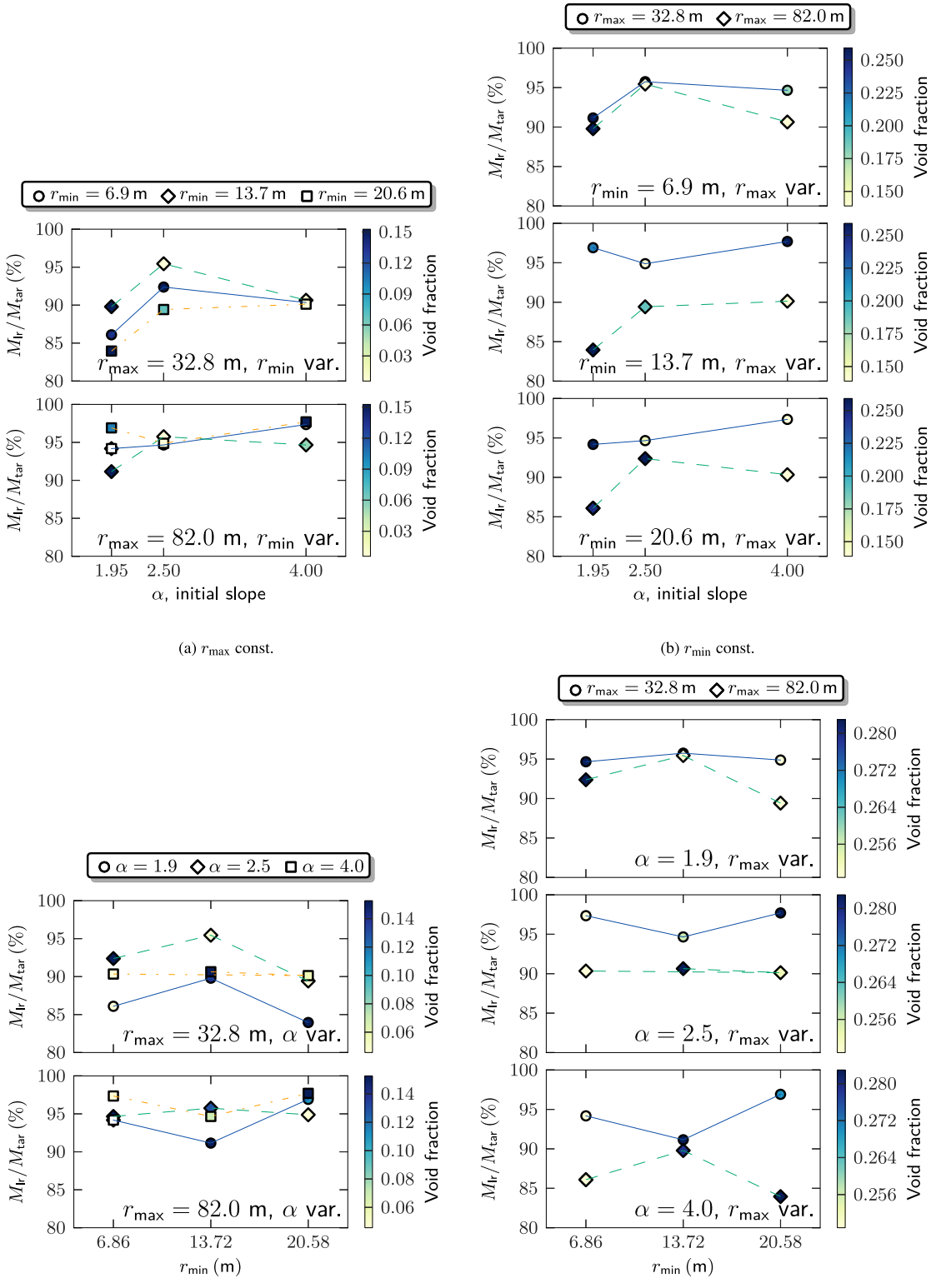

(a) r_{max} const.

(b) r_{min} const.

(c) r_{max} const.

(d) α const.

Figure 10. Mass of the largest remnant fraction after an impact of an $r_{imp} = 4$ m asteroid at $v_{imp} = 5.5\,km\,s^{-1}$ for different internal structures of the target. The targets have been formed as an $r_{tar} = 164$ m asteroid, the internal structure derived from a gravitational aggregate formed using a set of three parameters α, r_{min}, and r_{max} of the value matrix in Table 2. The individual error bar in relative mass is ±2 per cent (see Fig. 7 and Section,4.1). Each sub-figure shows the same set of data. Additional correlations can be found in Fig. 11.

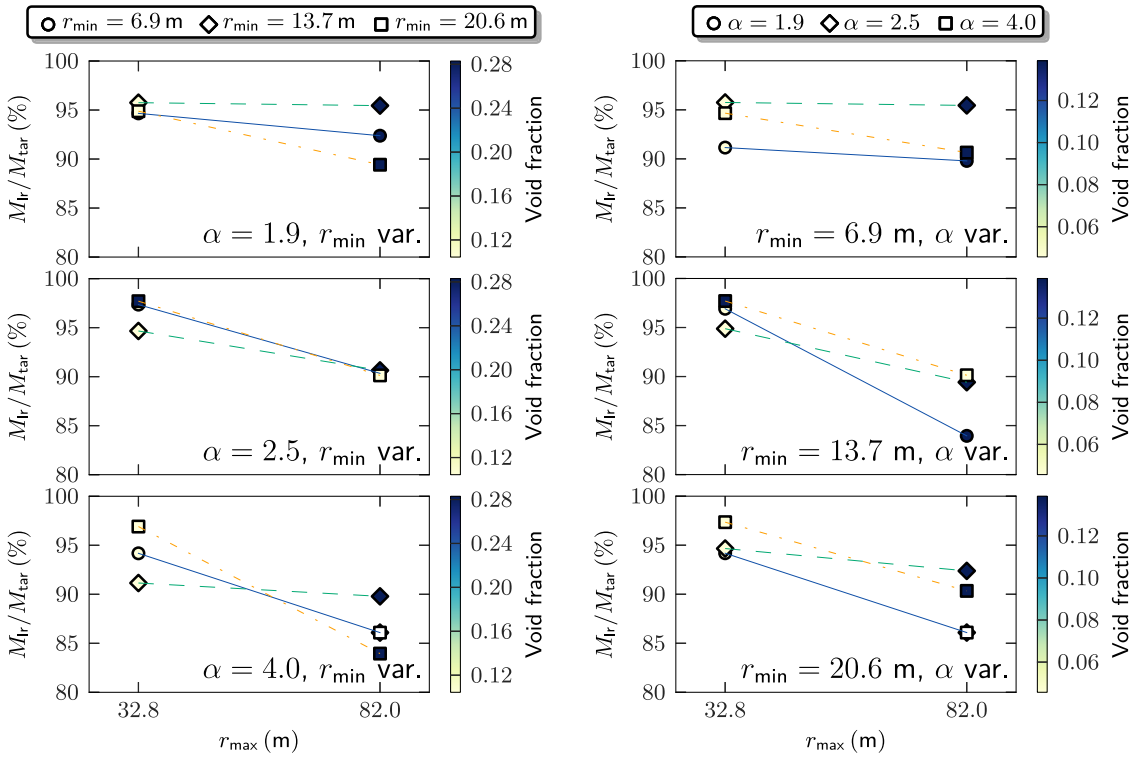

(a) α const. (b) r_{min} const.

Figure 11. As in Fig. 10, mass of the largest remnant fragment of the set of internal configurations given by Table 2.

resembles more of a solid body with randomly distributed voids, as the small pebbles fill the space between the large pebbles evenly.

The slope α seems to have no clear effect on the strength (Figs 10a and b): only a slight increase of strength when α is changed from $\alpha = 1.95$ to $\alpha = 4.00$ is observed.

The lower cut-off radius r_{min} seems to have no clear effect on M_{lr} (Fig. 10c and d): While for $r_{max} = 82$ m the strength increases with r_{min}, and for $r_{max} = 32$ m it decreases, this effect is small and not significant.

A larger upper cut-off radius r_{max} results in less resistance to disruption (Figs 11a and b): This is not an effect of the increasing size of the pebbles, but rather by the correlation of void space and r_{max} (See Fig. 9).

A lower cut-off radius of $r_{min} = 6.9$ m results in an insensitivity to the upper cut-off radius r_{max} (Fig. 11a, upmost panel): The unconnected void space with many small pebbles of only 1/24 of the asteroid's radius behaves like a solid material with random porosity, indicating that a lower cut-off radius of $r_{min} = 6.9$ m is too small to represent an asteroid model of loosely bound rubble. This is just a factor 2.7 larger than the smoothing length $h = 2.54$ m that limits the resolution of our simulation. A possible solution could be not to assume void space between the pebbles, but to fill it with a highly porous material described using a continuum material model or porous media.

In summary, we see the only clear correlation between strength and void fraction. Therefore, exact choice of the arbitrary parameters α, r_{min}, and r_{max} does not significantly influence the outcomes of our simulations in a direct way, and no physical explicit derivation of these parameters is needed.

For a lower cut-off pebble radius of $r_{min} = 6.9$ m, the model becomes insensitive to the upper cutoff radius r_{max}. This is most likely an effect of chosen resolution, governed by the smoothing length $h = 2.54$ m. We see, that for a rubble pile representation r_{min} has to be chosen as $r_{min} > 3 \times h$.

The main mechanism is the amount of the bulk porosity given by connected voids rather than single void cells inside the pebbles. If most of the porosity is given by connected void space, the pebbles themselves are more solid. The data point in Fig. 9 created using the model parameters $\alpha = 1.95$, $r_{min} = 20.58$ m and $r_{max} = 82$ m with a void fraction of 0.283, contains only 1.7 per cent of porosity inside the pebbles, as the bulk porosity of the target is fixed to $P_b = 30$ per cent. This is also the weakest model in the comparison, with a mass of the largest remnant fragment of $M_{lr}/M_{tar} = 83.95$ per cent. Like a solid asteroid, the disruption energy threshold Q^*_S for solid pebbles is lower than for a porous one, resulting in easier shattering of the pebbles that form the asteroid and causes a larger fraction of the mass to be excavated, and, therefore, a lower mass of the largest remnant fragment M_{lr}.

6 SUMMARY

The explicit modelling of the inner structure in rubble pile asteroids when simulating impact events is not only important to support abstract material models for brittle materials, but might also help us to understand the interior of asteroids from observing surface features such as depressions, impact craters or hill-like structures. The exact distribution of the void space that asteroids with high bulk porosities must contain – up to 60 per cent – is not known. Are there cavities inside rubble pile asteroids, as the series of aligned crater-like features on Šteins (Keller et al. 2010) might suggest?

This paper proposes a new way to create simulants for rubble pile asteroids, starting at the formation phase. In our model, the interior of a rubble pile asteroid is an agglomerate of spherical pebbles following a size distribution governed by a power law. This is only the first approach and an arbitrary choice, but supported by the size distributions observed in collisionally evolved populations (Dohnanyi 1971) and observations of asteroid families (e. g. Gladman et al. 2009). The pebble size distribution used to form the gravitational aggregate includes three free parameters: the power-law slope α, and the cut-off radii $r_{\rm min}$ and $r_{\rm max}$. All these parameters are hard to constrain by observational evidence. Therefore, this paper aims to determine the sensitivity of the impact outcomes on the choice of these parameters by running a series of test simulations.

The choice of the parameters used to form the gravitational aggregate does not appear to have a great influence on the outcome of the collision. The only direct correlation observable is to the void fraction, the void space in between the pebbles. If there is a higher void fraction, and therefore a higher fraction of connected voids inside the asteroid as opposed to unconnected void single cells, the 'strength' of the asteroid decreases as shown by the decreasing mass of the largest remnant fragment in Fig. 9. The void fraction is only indirectly controlled by the parameters of our model, and entangled in all three of them. For this reason, direct conclusions on the influence of the three model parameters are not straightforward. However, this does mean that a priori knowledge of the size distribution of the component parts of a rubble pile is not necessary to use our technique to simulate rubble pile asteroids in impact experiments. This means we can use a generic rubble pile model to study the outcomes of different collisions, without concern that our experiment is influenced by assumptions about the precise internal structure.

The lower cut-off limit is seen to be dependent on the chosen simulation resolution, given by the SPH smoothing length h. For values of $r_{\rm min} < 3 \times h$, the exact distribution of pebbles does not influence the result any more, and is undistinguishable from randomly distributed voids.

The main effect of our model is an overall strengthening of the asteroids' resistance against collisional disruption compared to a non-porous asteroid, as seen in the higher disruption energy threshold Q^*_S for these models (Fig. 8). This effect is explained by the energy needed to compress the voids and has been observed before (Holsapple 2009), and the values for Q^*_S found are in agreement with scaling laws derived by Jutzi et al. (2010a), while the generalized scaling law for the gravitational disruption regime by Leinhardt & Stewart (2011) can not be applied. The next step, using our rubble pile models to test how changes in the interior configuration due to impacts can influence surface features, will be the subject of a future paper.

ACKNOWLEDGEMENTS

We thank the referee, Dr Donald G. Korycansky, for helpful comments that improved this paper. This work was supported by funding of the University of Kent and the Max Planck Society in the framework of the International Max Planck Research School for Solar System Science.

REFERENCES

Abe S. et al., 2006, Science, 312, 1344
Ansys Inc, 2012, Autodyn User Manual 14.5 edn. Canonsburg, Pennsylvania, USA
Beitz E., Güttler C., Weidling R., Blum J., 2012, Icarus, 218, 701
Benavidez P. G., Durda D. D., Enke B. L., Bottke W. F., Nesvorný D., Richardson D. C., Asphaug E., Merline W. J., 2012, Icarus, 219, 57
Benz W. W., 2000, Space Sci. Rev., 92, 279
Benz W. W., Asphaug E., 1999, Icarus, 142, 5
Besse S., Lamy P. L., Jorda L., Marchi S., Barbieri C., 2012, Icarus, 221, 1119
Burbine T. H., Meibom A., Binzel R. P., 1996, Meteorit. Planet. Sci., 31, 607
Carry B., 2012, Planet. Space Sci., 73, 98
Collins G. S., Melosh H. J., Ivanov B. A., 2004, Meteorit. Planet. Sci., 39, 217
Davis D. R., Durda D. D., Marzari F., Campo Bagatin A., Gil-Hutton R., 2003, in Bottke W. F., Cellino A., Paolicchi P., Binzel R. P., eds, Asteroids III. University of Arizona Press, p. 545
Dohnanyi J. S., 1971, in Gehrels T., ed., IAU Colloq. 12, Physical Studies of Minor Planets. Tucson, AZ, p. 263
Elbeshausen D., Wünnemann K., Collins G. S., 2009, Icarus, 204, 716
Faraud M., Destefanis R., Palmieri D., Marchetti M., 1999, Int. J. Impact Eng., 23, 249
Farinella P., Paolicchi P., Zappalà V., 1982, Icarus, 52, 409
Geretshauser R. J., Speith R., Kley W., 2011, A&A, 536, A104
Gladman B. J. et al., 2009, Icarus, 202, 104
Grüneisen E., 1912, Ann. Phys., Lpz., 355, 257
Hayhurst C. J., Clegg R. A., 1997, Int. J. Impact Eng., 20, 337
Holsapple K. A., 2009, Planet. Space Sci., 57, 127
Ivanov B. A., Deniem D., Neukum G., 1997, Int. J. Impact Eng., 20, 411
Jorda L., Lamy P. L., Gaskell R. W., Kaasalainen M., Groussin O., Besse S., Faury G., 2012, Icarus, 221, 1089
Jutzi M., Michel P. P., Benz W. W., Richardson D. C., 2010a, Icarus, 207, 54
Jutzi M., Michel P. P., Benz W. W., 2010b, A&A, 509, L2
Keller H. U. et al., 2010, Science, 327, 190
Kothe S., Blum J., Weidling R., Güttler C., 2013, Icarus, 225, 75
Kresak L., 1976, Astron. Inst. Czech., 28, 65
Kwiatkowski T., 2010, A&A, 509, A95
Leinhardt Z. M., Stewart S. T., 2011, ApJ, 745, 79
McQueen R. G., Marsh S. P., Fritz J. N., 1967, J. Geophys. Res., 72, 4999
Marsh S. P., 1980, Lasl Shock Hugoniot Data. Univ. California Press, California
Michel P. P., Benz W. W., Tanga P., Richardson D. C., 2002, Icarus, 160, 10
Michel P. P., Benz W. W., Richardson D. C., 2004, Icarus, 168, 420
Michikami T. et al., 2008, in Earth Planets Space, 60, 13
Michikami T., Nakamura A. M., Hirata N., 2010, Icarus, 207, 277
Mie G., 1903, Ann. Phys., Lpz., 316, 657
Pierazzo E. et al., 2008, Meteorit. Planet. Sci., 43, 1917
Pravec P., Harris A. W., Michalowski T., 2002, in Bottke W. F., Cellino A., Paolicchi P., Binzel R. P., eds, Asteroids III. Univ. Arizona Press, Tucson, AZ, p. 113
Price M. C., Kearsley A. T., Burchell M. J., Howard L. E., Hillier J. K., Starkey N. A., Wozniakiewicz P. J., Cole M. J., 2012, Meteorit. Planet. Sci., 47, 684
Rein H., Liu S. F., 2012, A&A, 537, A128
Richardson D. C., Leinhardt Z. M., Melosh H. J., Bottke W. F. J., Asphaug E., 2003, in Bottke W. F., Cellino A., Paolicchi P., Binzel R. P., eds, Asteroids III. Univ. Arizona Press, Tucson, AZ, p. 501
Rozitis B., MacLennan E., Emery J. P., 2014, Nature, 512, 174
Saito J. et al., 2006, Science, 312, 1341
Schenk P. M., Asphaug E., McKinnon W. B., Melosh H. J., Weissman P. R., 1996, Icarus, 121, 249
Tanga P., Cellino A., Michel P. P., Zappalà V., Paolicchi P., dell'Oro A., 1999, Icarus, 141, 65
van Houten C. J., van Houten-Groeneveld I., Herget P., Gehrels T., 1970, A&AS, 2, 339
Weidling R., Güttler C., Blum J., 2012, Icarus, 218, 688

This paper has been typeset from a TEX/LATEX file prepared by the author.